Transport in a magnetic field modulated graphene superlattice

2010 J. Phys.: Condens. Matter 22 015302

(http://iopscience.iop.org/0953-8984/22/1/015302)

J. Phys.: Condens. Matter **22** (2010) 015302 (5pp) doi:10.1088/0953-8984/22/1/015302

Transport in a magnetic field modulated graphene superlattice

Yu-Xian Li

College of Physics, Hebei Normal University, Shijiazhuang 050016, People's Republic of China
and
Hebei Advanced Film Laboratory, Shijiazhuang 050016, People's Republic of China

Received 21 September 2009, in final form 14 November 2009
Published 8 December 2009
Online at stacks.iop.org/JPhysCM/22/015302

Abstract

Using the transfer matrix method, we study the transport properties through a magnetic field modulated graphene superlattice. It is found that the electrostatic barrier, the magnetic vector potential, and the number of wells in a superlattice modify the transmission remarkably. The angular dependent transmission is blocked by the magnetic vector potential because of the appearance of the evanescent states at certain incident angles, and the region of Klein tunneling shifts to the left. The angularly averaged conductivities exhibit oscillatory behavior. The magnitude and period of oscillation depend sensitively on the height of the electrostatic barrier, the number of wells, and the strength of the modulated magnetic field.

1. Introduction

Graphene and graphene-based microstructures have recently attracted strong interest for potential nano-electronic applications due to their excellent carrier transport properties [1–4]. Graphene has a honeycomb lattice of carbon atoms. The quasiparticles in graphene have a band structure in which electron and hole bands touch at two points in the Brillouin zone [5, 6]. At these Dirac points, the quasiparticles obey the massless Dirac equation, which leads to a linear dispersion relation $\varepsilon_k = vk$ (with a characteristic velocity $v \approx 10^6$ m s^{-1}). The presence of such quasiparticles in graphene can provide us with an experimental test for the Klein paradox [4]. Klein tunneling predicts that the electron can pass through the high potential barrier to approach perfect transmission in contrast to conventional nonrelativistic tunneling where the transmission probability exponentially decays with increasing barrier height [7–9].

Several graphene-based devices have been designed and their transport properties studied. In double barrier (well) graphene resonant tunneling structures [10], the massless charge carriers can be confined by means of electrostatic potential, due to the wavevector dependent suppression of the electron–hole conversion at the potential barriers. Electron states in the wells and hole states in the barriers give rise to resonant features, which strongly influence the ballistic conductance. Another interesting structure is a graphene superlattice [11]. The angularly averaged conductivities in a graphene superlattice can be controlled by changing the structure parameters even if Klein tunneling exists.

It was found very recently that a new phenomenon appears in a graphene structure with magnetic barriers [12–14]. The Landau levels broaden into bands and the level width oscillates with the magnetic field. The Dirac fermions can transmit perfectly through a classically forbidden region while confined by the magnetic barrier. For a graphene monolayer system modulated by two ferromagnetic electrodes, the transmission can be blocked by the magnetic–electric barrier, resulting in a tremendous magnetoresistance ratio [15]. However, the effects of magnetic field modulation on the graphene multiple quantum wells or superlattice have not been investigated. In this work, we explore the transport properties of the graphene superlattice under the modulation of the magnetic field. Different transmission properties and conductivity are presented with the magnetic field modulation.

2. Model and method

The system under consideration is a monolayer graphene superlattice. The schematic potential profiles for the double barriers and superlattice are shown in figures 1(a) and (b). The growth direction is taken as the x axis, which is termed the superlattice axis. The magnetic field is applied along the z direction perpendicular to the graphene (x, y) plane. In this paper, we consider a series of magnetic δ-function barriers that alternate in sign. This model can be realized experimentally

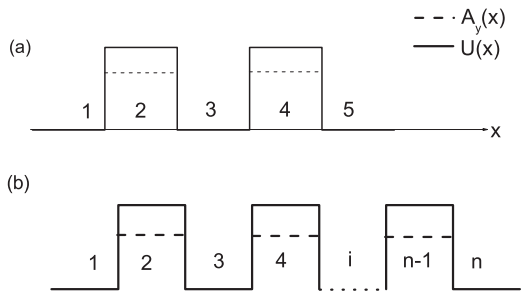

Figure 1. Potential profile of quasiparticle transport in the monolayer graphene superlattice (a) with double barriers (one well) and (b) with $(n-1)/2$ barriers ($(n-3)/2$ wells).

by depositing ferromagnetic strips on top of a graphene layer or putting the graphene layer on a periodically structured substrate [16]. Within the Landau gauge, the vector potential $A(x)$ is a periodic array of step functions. A square shaped barrier potential with height U_0 can be taken for the electric potential created by either gate. Due to the difference in Fermi energy and band structure between two monolayer graphene strips, the potential profile of the system is a multiple quantum well (barrier) structure, given by

$$V(x) = \begin{cases} U_0, & \text{in barrier,} \\ 0, & \text{in well.} \end{cases} \tag{1}$$

We consider the monolayer graphene within the single electron approximation; the low energy excitations are described by the Dirac-type equation

$$[v_F \sigma \cdot (\mathbf{p} + e\mathbf{A}) + V_x \sigma_0]\Psi = E\Psi, \tag{2}$$

where $v_F \approx 0.86 \times 10^6$ m s^{-1} is the Fermi velocity of the structure, σ is the Pauli matrix, $\mathbf{p} = (p_x, p_y)$ is the electron momentum, $\mathbf{A}$ is the vector potential with the form $\mathbf{A} = [0, A_y, 0]$, and σ_0 is the 2×2 unit matrix.

Because the system in our model is homogeneous along the y direction, the transverse wavevector k_y is conserved. The solution of equation (2) for a given incident energy E can be written as

$$\Psi_w = \mathrm{e}^{\mathrm{i}k_y y}\left[a_i \mathrm{e}^{\mathrm{i}k_x x}\begin{pmatrix} 1 \\ \frac{k_x + \mathrm{i}k_y}{E} \end{pmatrix} + b_i \mathrm{e}^{-\mathrm{i}k_x x}\begin{pmatrix} 1 \\ \frac{-k_x + \mathrm{i}k_y}{E} \end{pmatrix}\right] \tag{3}$$

in the well and

$$\Psi_b = \mathrm{e}^{\mathrm{i}k_y y}\left[c_i \mathrm{e}^{\mathrm{i}k_x x}\begin{pmatrix} 1 \\ \frac{k_x + \mathrm{i}q}{(E-U_0)} \end{pmatrix} + d_i \mathrm{e}^{-\mathrm{i}k_x x}\begin{pmatrix} 1 \\ \frac{-k_x + \mathrm{i}q}{(E-U_0)} \end{pmatrix}\right] \tag{4}$$

in the barrier. Here, $q = k_y + A_y$, and k_x is the longitudinal wavevector satisfying

$$k_x^2 + (k_y + A_y)^2 = (E - U_0)^2. \tag{5}$$

Using the continuity of the wavefunction at the boundaries and the transfer matrix method, the coefficients in equations (3) and (4) can be solved, and the transmission probability can be calculated $T = T(E, k_y)$.

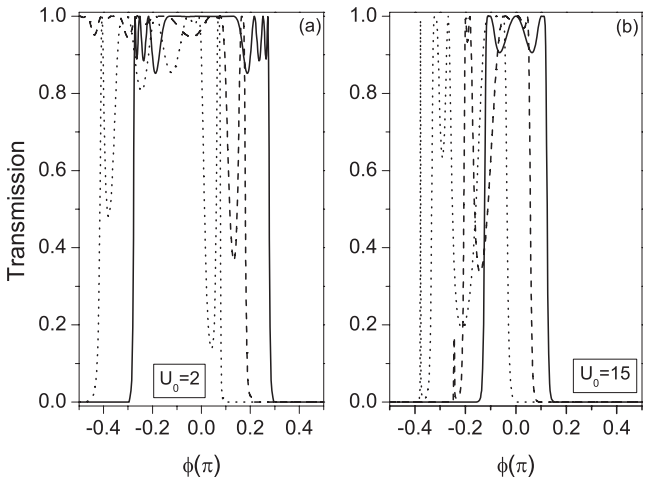

Figure 2. Transmission probability of electrons through double barrier (single well) structures as a function of the incident angle with $U_0 = 2E_0$ (a) and $U_0 = 15E_0$ (b). $E_F = 10E_0$; solid, dashed, and dotted lines correspond to $B = 0$, $2B_0$, and $5B_0$, respectively.

Based on the Landauer–Büttiker conductance formula [17], the ballistic conductance in this system can then be written as

$$G(E_F) = (4e^2/h)\int_{-E_F}^{E_F} T(E_F, k_y)\frac{\mathrm{d}k_y}{2\pi/L_y} \tag{6}$$

$$= G_0 \int_{-\pi/2}^{\pi/2} T(E_F, E_F \sin\phi)\cos\phi\,\mathrm{d}\phi, \tag{7}$$

where $L_y \gg L$ is the sample size along the y direction, ϕ is the incident angle relative to the x direction, $\phi = \arccos(k_x/E_F)$, and $G_0 = 2e^2 E_F L_y/(\pi h)$ is taken as the conductance unit.

3. Results and analysis

In the present model, the strength of the local magnetic field, $l_B = \sqrt{\hbar/eB}$, and the energy, $E_0 = \hbar v_F/l_B$, are taken as the units of the length and energy, respectively. For a realistic value $B_0 = 0.1$ T, we have $l_0 = 811$ Å and $E_0 = 7.0$ meV [15]. In the following numerical calculation, the widths of the barriers and the wells are set at 1. The incident energy is fixed at $E = 10E_0$, the magnetic field B is taken as 0, $2B_0$, or $5B_0$ for different transmission properties.

We first study the double barrier (one well) structure. Figures 2(a) and (b) show the transmission versus the incident angle with different magnetic fields. Perfect transport appears very clearly for the case of normal incidence, which is Klein tunneling. Increasing the height of the barrier, the region of resonant tunneling decreases. When the magnetic field is applied, we can see from figures 2(a) and (b) that the location of the transmission peak with a finite width changes from $k_y = 0$ to $k_y = -B$ (here $B = A_y$). The shape of the transmission curve shifts left and the incident direction at which Klein tunneling occurs changes with the magnetic field; as a result the transmission is no longer symmetric about the incident angle. This can be understood as follows. From equation (5) we can see that when the magnetic vector potential and the electrostatic barrier satisfy $|k_y + B| > |E - U_0|$, the

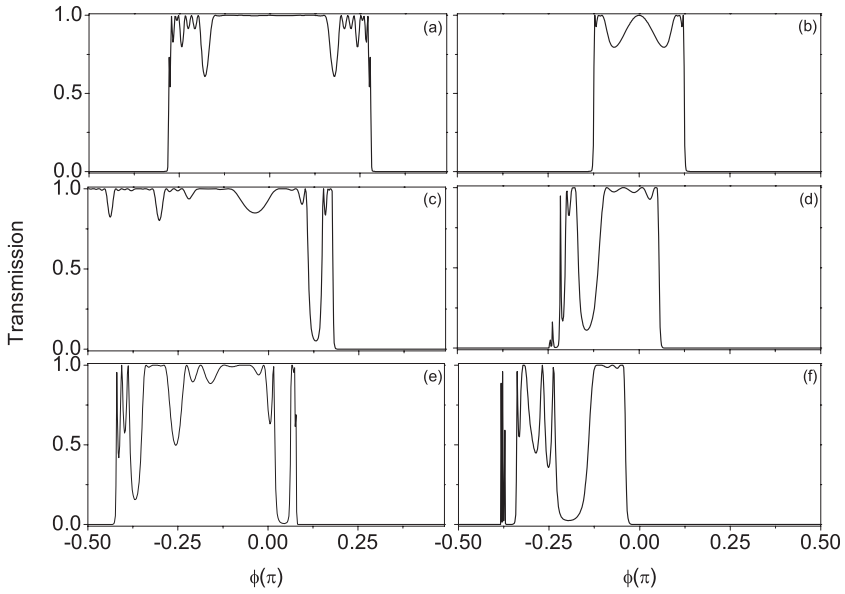

Figure 3. Transmission probability of electrons through three-well structures with $U_0 = 2E_0$ ((a), (c), and (e)) and $U_0 = 15E_0$ ((b), (d), and (f)). The magnetic field $B = 0$ for (a) and (b), $B = 2B_0$ for (c) and (d), and $B = 5B_0$ for (e) and (f). $E_F = 10E_0$.

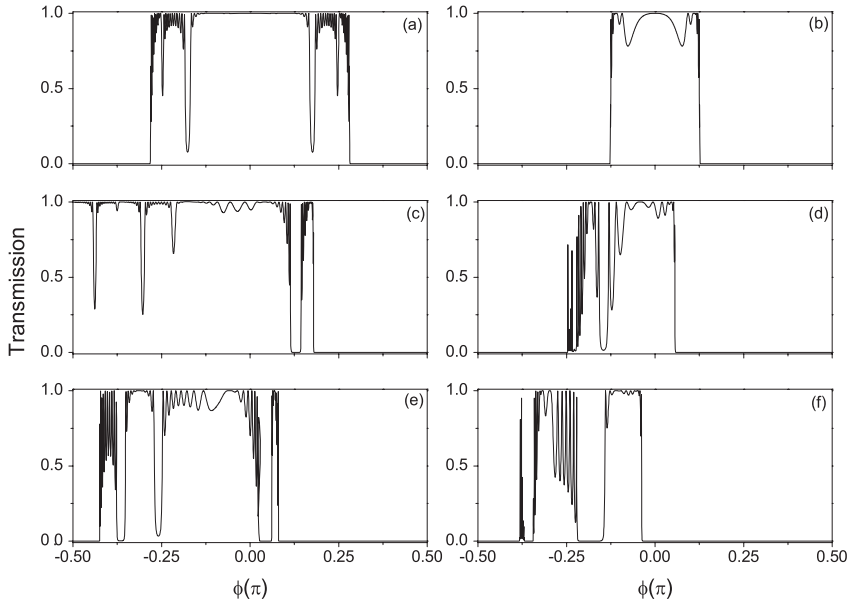

Figure 4. Transmission probability T of electrons through ten-well structures with $U_0 = 2E_0$ ((a), (c), and (e)) and $U_0 = 15E_0$ ((b), (d), and (f)). The magnetic field $B = 0$ for (a) and (b), $B = 2B_0$ for (c) and (d), and $B = 5B_0$ for (e) and (f). $E_F = 10E_0$.

evanescent states appear in the magnetic field regions and the transmission is generally weak as the decaying length of the evanescent states is shorter than the vector potential width; as a result, the transmission is blocked by the magnetic field when the incident angle exceeds a critical value.

The transmission properties for the graphene superlattice with three wells are plotted in figure 3. The electrons reflect and transmit through the interface of the barrier and the well, and compared with the case of a single well, more conductivity peaks appear with increasing well number. The number of wells plays an important role in anisotropic transmission even for the graphene superlattice. The curve of the transmission shifts to the left by modulation of the magnetic field. Because the propagating states only appear in the magnetic vector potential regions $|k_y + B| < |E_F - U_0|$, when the Fermi energy E_F is bigger than the electrostatic barrier U_0, that means

$$U_0 - E_F - B < k_y < E_F - U_0 - B. \tag{8}$$

We can see from figures 3(a), (c), and (e) that, with the applied magnetic field increasing, the positive critical value of the incident angle becomes small and the region of electron tunneling shifts to the left. On the other hand, the negative critical angle is determined by competition between the magnetic vector potential and the electrostatic barrier

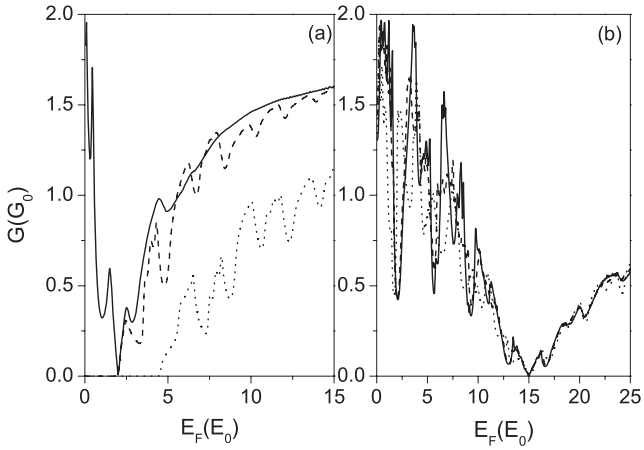

Figure 5. Conductivity as a function of the Fermi energy E_F for three-well structures with $U_0 = 2E_0$ (a) and $U_0 = 15E_0$ (b). Solid, dashed, and dotted lines corresponding to $B = 0$, $2B_0$, and $5B_0$, respectively.

$U_0 - E_F - B$. For example, with $U_0 = 2E_0$, $B = 5B_0$ in figure 3(e), transmission is forbidden when the incident angle exceeds the positive critical angle $\phi = 0.1\pi$ or is below another critical negative value $\phi = -0.4\pi$. When the magnetic vector potential and the electrostatic barrier have the same values, $-E_F < k_y$ in equation (8) (see figure 3(c)) the transmission appears for all negative incident angles. But for the case of $U_0 > E$, electron tunneling through the electrostatic barrier acts as the dominated transport process. From figures 3(b), (d), and (f) it is found that the higher electrostatic barrier holds back electron transport through the structure, but in regions of negative incident angle the applied magnetic barrier improves it and widens the tunneling spectrum. The angular dependent transmission in a ten-well graphene superlattice is also calculated and the results are shown in figure 4. Because the electrons experience a longer well–barrier interface, more reflection and transmission happen. Compares with the case of the three-well structure, the magnetic barrier does not modify the region of the transmission, but increases the number of transmission peaks.

The angular averaged conductivities are related to the well (barrier) structure of the graphene superlattice. We calculated the angular averaged conductivities in a three-well superlattice with different magnetic fields and the results are plotted in figure 5. For the case of $U_0 = 2E_0$ we can see that, without the magnetic field modulation, the conductivity exhibits oscillatory behavior but decreases when the Fermi energy is less than the electrostatic barrier ($E_F < U_0$) and then increases when the Fermi energy increases. When the Fermi energy equals the electrostatic barrier, from equation (5), $k_x^2 + (k_y + A_y)^2 = 0$, transmission is forbidden and the angular averaged conductivity is zero. With the magnetic field applied, the oscillation of the angular averaged conductivities becomes stronger but with a small magnitude oscillation. The magnitude and period of the oscillation depend sensitively on the magnetic field. The magnetic vector potential quickens the oscillatory frequency of the conductivities. It is interesting to note that the angular averaged conductivities are completely compressed when the Fermi energy is smaller than the magnetic field. In contrast, for a higher electrostatic barrier, i.e. $U_0 = 15E_0$ in figure 5(b), the angular averaged conductivities decrease with oscillation as the Fermi energy increases, and then become zero when the Fermi energy equals the electrostatic barrier and then increases again. When a magnetic field was applied, the amplitude of the oscillation became small.

Now we discuss the effect of the magnetic field on the conductivities in graphene superlattices with different well numbers. Figure 6 shows conductivity as a function of the

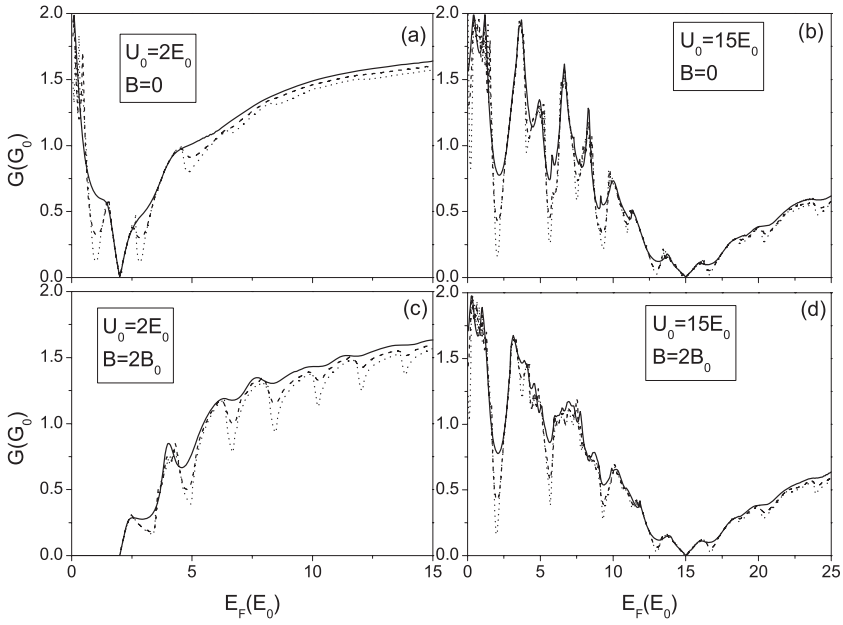

Figure 6. Conductivity as a function of the Fermi energy with different barrier heights and magnetic fields. Solid, dashed, and dotted lines correspond to one-, three-, and ten-well structures, respectively.

Fermi energy E_F with various numbers of wells. The solid line, dashed line, and dotted line correspond to the cases with one, three, and ten wells, respectively. $U_0 = 2E_0$ for figures 6(a) and (c) and $U_0 = 15E_0$ for figures 6(b) and (d). The electrostatic potential clearly modifies the conductivity. The oscillation period does not change, the oscillation magnitudes are tuned largely with the increase in well number. Comparing figures 6(a) and (c), we can see that the oscillation becomes quicker and the magnitude becomes wider because of the magnetic field not only for the case of the one-well structure but also for the ten-well superlattice. As to the higher electrostatic potential, in figures 6(b) and (d) the behavior of the conductivities varies in a more complicated way under the applied magnetic field. The magnitude and period of oscillation depend sensitively on the electrostatic barrier and the modulation of the magnetic field.

4. Summary

In summary, based on the transfer matrix method we have investigated the angle dependent transmission and the angle averaged conductivities through graphene superlattices under modulation of the magnetic field. It is found that the transmission probability is directly related to the number of the wells and the height of the potential, even if Klein tunneling exists in the graphene structure. The magnetic vector potential modulation blocks electron transport and shifts the region of Klein tunneling. The angle averaged conductivities show oscillatory behavior with increasing well number. As a function of the Fermi energy, the conductivities oscillate and decrease to zero when the Fermi energy equals the electrostatic barrier and then increase again with increasing Fermi energy. Thus, the transport properties in a graphene superlattice can be controlled by the magnetic vector potential and the electrostatic barrier.

Acknowledgments

This work was supported by National Natural Science Foundation of China (grant no. 10974043) and Hebei Province Natural Science Foundation of China (grant no. A2009000240).

References

[1] Novoselov K S, Geim A K, Morozov S V, Jiang D, Zhang Y, Dubonos S V, Grigorieva I V and Firsov A A 2004 *Science* **306** 666
[2] Berger C, Song Z M, Li X B, Wu X S, Brown N, Naud C, Nato D, Li T B, Hass J, Marchenkov A N, Conrad E H, First P N and de Heer W A 2006 *Science* **312** 1191
[3] Zhang Y, Tan Y W, Stormer H L and Kim P 2005 *Nature* **438** 201
[4] Katsnelson M I, Novoselov K S and Geim A K 2006 *Nat. Phys.* **2** 620
[5] Wallace P R 1947 *Phys. Rev.* **71** 622
[6] Ando T 2005 *J. Phys. Soc. Japan* **74** 777
[7] Su R K, Siu G C and Chou X 1993 *J. Phys. A: Math. Gen.* **26** 1001
[8] Dombey N and Calogeracos A 1999 *Phys. Rep.* **315** 41
[9] Krekora P, Su Q and Grobe R 2004 *Phys. Rev. Lett.* **92** 040406
[10] Pereira J M Jr, Vasilopoulos P and Peeters F M 2007 *Appl. Phys. Lett.* **90** 132122
Pereira J M Jr, Mlinar V, Peeters F M and Vasilopoulos P 2006 *Phys. Rev.* B **74** 045424
[11] Bai C and Zhang X 2007 *Phys. Rev.* B **76** 075430
[12] De Martino A, Dell'Anna L and Egger R 2007 *Phys. Rev. Lett.* **98** 066802
[13] Tahir M and Sabeeh K 2008 *Phys. Rev.* B **77** 195421
[14] Xu H, Heinzel T, Evaldsson M and Zozoulenko I V 2008 *Phys. Rev.* B **77** 245401
[15] Zhai F and Chang K 2008 *Phys. Rev.* B **77** 113409
[16] Masir M R, Vasilopoulos P and Peeters F M 2009 *New J. Phys.* **11** 095009
[17] Büttiker M, Imry Y, Landauer R and Pinhas S 1985 *Phys. Rev.* B **31** 6207
Büttiker M 1986 *Phys. Rev. Lett.* **57** 1761